High-field magnetic circular dichroism in ferromagnetic InMnSb and InMnAs: Spin-orbit-split hole bands and *g* factors

M. A. Meeker, B. A. Magill, and G. A. Khodaparast*
Department of Physics, Virginia Tech, Blacksburg, Virginia 24061, USA

D. Saha and C. J. Stanton
Department of Physics, University of Florida, Gainesville, Florida 32611, USA

S. McGill
National High Magnetic Field Laboratory, Tallahassee, Florida 32310, USA

B. W. Wessels
Material Research Center, Northwestern University, Evanston, Illinois 60208, USA
(Received 26 May 2015; revised manuscript received 15 July 2015; published 18 September 2015)

Carrier-induced ferromagnetism in magnetic III-V semiconductors has opened up several opportunities for spintronic device applications as well as for fundamental studies of a material system in which *itinerant* carriers interact with the localized spins of magnetic impurities. In order to understand the hole mediated ferromagnetism, probing the band structure in these material systems is crucial. Here we present magnetic circular dichroism (MCD) studies on MOVPE grown InMnSb and InMnAs, both with the Curie temperatures above 300 K. The measurements were performed on samples with different Mn contents with the excitation energy tuned from 0.92–1.42 eV and external magnetic fields up to 31 T. The large *g* factors in these systems allow us to measure the MCD at relatively high temperatures (190 K). These measurements are compared with MCD calculations based on an eight-band Pidgeon-Brown model, which is generalized to include the coupling between the electron/hole and the Mn spin in a ferromagnetic state. Comparison of the observed MCD with the theoretical calculations provides a direct method to probe the band structure including the temperature dependence of the spin-orbit split-off gap and *g* factors, and to estimate the *sp-d* coupling constants.

DOI: 10.1103/PhysRevB.92.125203 PACS number(s): 75.50.Pp, 78.20.Ls, 78.47.−p, 78.66.Fd

I. INTRODUCTION

Narrow gap ferromagnetic semiconductors (NGFS) such as InMnAs and InMnSb offer promising potential for applications in infrared spin photonics, memory storage, and spin transport devices [1–4]. Compared to GaMnAs [5], NGFS have smaller band gaps, larger *g* factors, and spin-orbit coupling [6,7], and much higher electron and hole mobilities. The narrow gap materials are also more interesting and difficult to treat theoretically since there is strong band mixing between the conduction and valence bands, unlike GaAs where the conduction and valence bands can be treated separately [8,9].

In the past, low-temperature molecular beam epitaxy (MBE) [1,2,10,11] techniques were nearly exclusively used to prepare NGFS; however, metal-organic vapor phase epitaxy (MOVPE) demonstrated that a single phase NGFS compound could be deposited at 500 °C, much higher than that used in MBE [12–14]. Furthermore, the MOVPE technique demonstrated that the films are ferromagnetic with a T_c above room temperature (RT) [12–14]. This is thought to be due to the fact that in MOVPE grown samples, there are local formations of Mn dimers, trimers, and tetramers [15,16], which lowers the hole density and the Fermi energy. As a result of a lower hole density in the MOVPE grown NGFS, an earlier study estimated that a larger average hole spin polarization, compared to the MBE grown structure, can be achieved [17]. This fact could be responsible for the higher T_c in the MOVPE grown structures. The record T_c of MBE grown GaMnAs is ∼178 K [18] and for MBE grown InMnSb and InMnAs the reported T_c measurements are <10 and <100 K, respectively [19–22].

The ferromagnetic films studied in this work, were grown on GaAs (100) substrates using atmospheric pressure MOVPE. These alloys were grown at a substrate temperature of 400 °C to 520 °C at a typical growth rate of 330 nm/hr [12,14,23]. The Mn concentration was determined by electron microprobe analysis. All four samples exhibit ferromagnetism with T_C between 330–400 K, as obtained from superconducting quantum interference device measurements.

In our InMnAs films, for Mn concentration equal to or larger than 8%, the ferromagnetism is mainly due to hexagonal MnAs clusters [24]. In the case of InMnSb for Mn contents larger than 15%, the temperature-dependent magnetization indicates that at least two magnetic phases are present, one with a nominal T_C of 300 K that is attributed to $MnAs_{1-x}Sb_x$ nanoprecipitates which form at the GaAs substrate interface, and a second with a $T_C > 400$ K that is attributed to hex-MnSb nanoprecipitates and to the InMnSb matrix [25,26]. On the other hand, in the samples studied here, the volume fraction of MnAs or MnSb precipitates, if present, is estimated to be below a volume fraction of 0.1%. As shown in Fig. 1, for our InMnSb with Mn = 10.7%, the structure is a single phase InMnSb.

In this work, we report on magnetic circular dichroism (MCD) studies. MCD is a powerful tool for studying ferromagnetic semiconductors where the *sp-d* coupling between

*Author to whom correspondence should be addressed: khoda@vt.edu

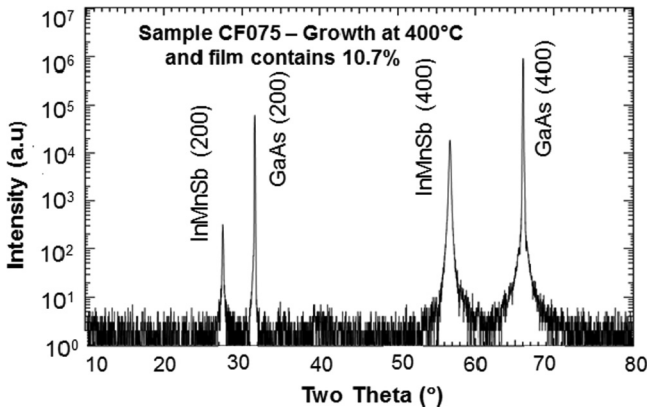

FIG. 1. The x-ray diffraction of InMnSb with 10.7% Mn demonstrating a single-phase structure. The sample is 500-nm-thick, grown on GaAs, and has a hole density of 1.3×10^{18} cm^{-3}.

the Mn ions and conduction and valence bands, as well as the band structure can be studied. Our MCD measurements at high magnetic fields were performed at various temperatures (15–190 K), external fields up to 31.25 T, and excitation energies ranging from 0.92–1.42 eV. Although our measurements were performed relatively far from the Γ point of InMnSb and InMnAs, the large external magnetic fields enhanced our resolution where several transitions, including the spin-orbit split-off (SO) to conduction-band (CB) transitions, were resolved [27]. Recent MCD studies in GaMnAs, in addition to several transport and magnetization measurements, have shown that the location of the Fermi level within the impurity band can play an important role in obtaining T_c [28]. Previous MCD studies on InMnAs and InMnSb aimed to probe the impurity band and the nature of the Mn *sp-d* interactions [15,16,19–21]. These measurements were performed at low magnetic fields [19–21,29], on MBE grown InMnSb structures with the $T_c \approx 10$ K [19–22,29] close to the band gap, or on MOVPE grown InMnAs with the T_c of ≈330 K, at energies ranging from 1.6 to 3.0 eV [15,16].

II. SAMPLES

The samples studied here were MOVPE grown InMnSb and InMnAs structures on GaAs substrates grown at Northwestern University, the details of the growth conditions were described in Refs. [12,14,23] and the characteristics of the samples are summarized in Table I.

TABLE I. Characteristics of the samples studied in this work. The samples are grown on GaAs substrates and in order to avoid damage to the samples, the T_c was not measured above 400 K.

Sample	Density cm^{-3}	Film Thickness nm	x %	Tc K
InMnAs (PTC017)	1.35×10^{18}	600	4	330
InMnAs(PTC015)	1.6×10^{18}	235	2	330
InMnSb(CF009)	2.2×10^{18}	200	4.7	400
InMnSb(CF075)	1.3×10^{18}	500	10.7	400

III. MCD MEASUREMENTS

Our MCD measurements were performed at the National High Magnetic Field Laboratory in Tallahassee, Florida, using the Split Florida-Helix magnet, allowing the temperature to vary between 15–190 K and fields up to 31.25 T. The excitation source was a Quartz Tungsten Halogen lamp with the emitted light being passed through a monochromator set to have a bandwidth of 5 nm. The light was polarized to 45° using a Glan-cube, and the polarization was altered between left- and right-handed circular polarization by a photo-elastic modulator at 50 KHz. The signal was transmitted through a fiber and detected by a Thorlabs InGaAs detector [PDA20CS]. In order to remove background signals, the MCD presented here is the difference in transmission between right- and left-handed circular polarizations, averaged over positive and negative fields, and normalized to the intensity of the lamp and the sample thickness: MCD $= \frac{\Delta T(B)-\Delta T(-B)}{2dI_0}$, where $T(B)$ is the magnetic field dependent transmission, B is the external magnetic field, d is the sample thickness, and I_0 is the incident intensity of the lamp. Here, the MCD measurements were presented only on the Mn-doped samples, where the films with no Mn demonstrated a reasonable signal to noise ratio of MCD, at the temperatures below 20 K, which could be related to more randomly distributed impurities in the *p*- and *n*-doped films. An earlier MCD study on MBE grown InMnSb was compared with a 1.52-mm-thick InSb wafer, available commercially, at 1.8 K [21]. In addition, in the case of the MCD study on the MBE grown InMnSb [21] (ranging from 1–5 μm), the dominating transitions were the intra-valence-band transitions from light to heavy holes. The MCD responses were insensitive to external magnetic fields, where both heavy- and light-hole bands shifted in the same direction with a changing external magnetic field. In this case [21], only the value of the valence-band exchange constant entered in the modeling of the MCD, while the influence of the conduction-band exchange parameter was not significant. Our MCD study, at high magnetic fields with the probe energy ranging from 0.92–1.42 eV, allowed us to examine the exchange coupling parameters both in the valence and conduction bands using the model described later in this paper.

A. InMnSb

Figure 2 shows a typical MCD trace for the two different InMnSb films. The MCD spectra display a broad positive background signal throughout the range as well as an oscillatory like behavior. The oscillations are not due to the Fabry-Perot interference, as shown in the inset of Fig. 2, no oscillatory pattern was observed for the transmission through the samples, at the same magnetic field. Previous MCD measurements on MBE grown InMnSb showed small peaks around 1000 nm (1.24 eV) [20,29] at low magnetic fields, while a different MCD study, has shown a relatively broad peak centered at ∼1250 nm (0.992 eV) [19].

In this study, the magnetic field dependence of the MCD response was measured and an example of the field dependence for CF009 (InMnSb with 4.7% Mn) is shown in Fig. 3. As the magnetic field increases, the amplitude of MCD increases and blue shifts in energy while the overall shape remains the same.

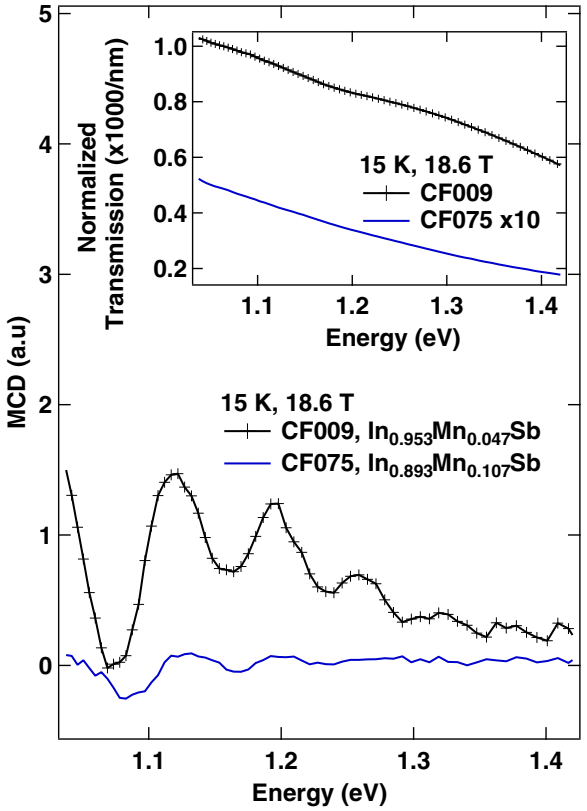

FIG. 2. (Color online) The MCD spectra of the two InMnSb structures with different Mn content. The oscillations in the MCD spectra are related to several interband transitions. As shown in the inset, the oscillations are not due to interference as they are absent in the transmission through the samples when the detected signal was not polarized.

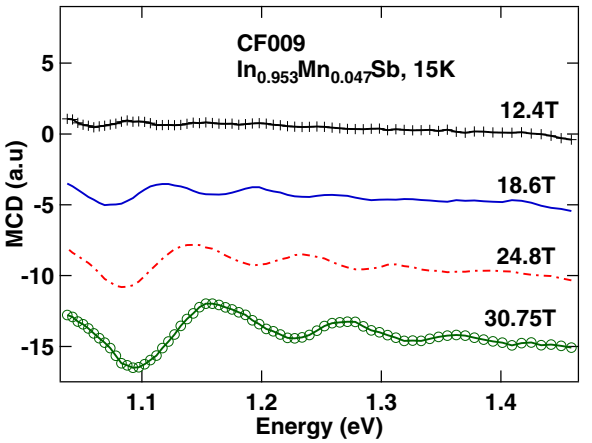

FIG. 3. (Color online) The Magnetic field dependence of the MCD spectra for the InMnSb (CF009, with Mn = 4.7%) at 15 K as a function of the excitation energies is presented here. The MCD is resolved more significantly at high fields where the blue shift is expected as a result of larger band splitting at higher fields. The peaks are shifted for clarity.

This fact can be described in a simple picture sketched in Fig. 4. As shown in panel (a), due to the Zeeman splitting, the spin degeneracy is lifted, and in this case shifting the $|HH\downarrow\rangle$ and $|LH\downarrow\rangle$ bands to a higher energy, as a result, the two spin states will be above the Fermi energy and can only have contributions to MCD transitions at higher energies. In Fig. 4(b), the density of states, for a quasi-one-dimensional system, is presented. As shown by the red dashed line, the net MCD can be extracted by taking the sum of the contributions from the HH and LH bands with different spins. When the magnetic field increases, the splitting of the bands become larger, and therefore the lowest-energy transition becomes higher in energy, possibly leaving those bands completely above the Fermi energy. This will result in reduced contributions from these states and increases the MCD signal until higher-energy effects, not shown here, such as the Landau levels, start to contribute. Our magnetic field dependence MCD measurements show a strong increase in the magnitudes and the expected blue shifts.

B. InMnAs

Figure 5 shows examples of MCD transitions for $In_{0.96}Mn_{0.04}As$ (blue) and $In_{0.98}Mn_{0.02}As$ (black) at ∼60 K and ∼31 T. The MCD response from both structures displays a similar pattern, with a small blue shift for the higher Mn

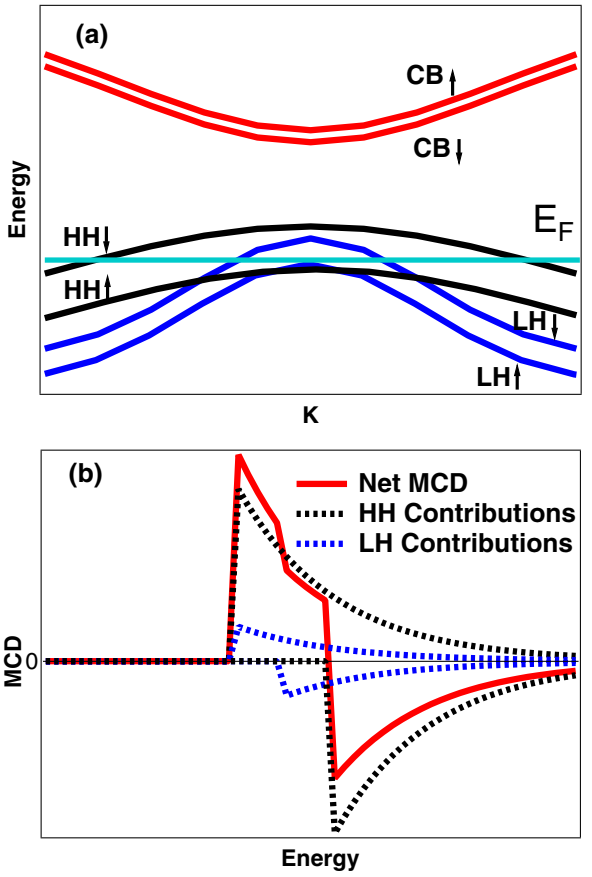

FIG. 4. (Color online) (a) A simplified picture of the band structure for a semiconductor in a magnetic field. The $|\downarrow\rangle$ spin states are partially above the Fermi energy, represented by the light blue line. (b) The density of states for a quasi-one-dimensional system where a bulk structure is placed in an external magnetic field. The contributions to the MCD can be seen in (b), with the partial contributions arising from regions identified by the dashed lines, and the full contribution from regions identified by the solid line.

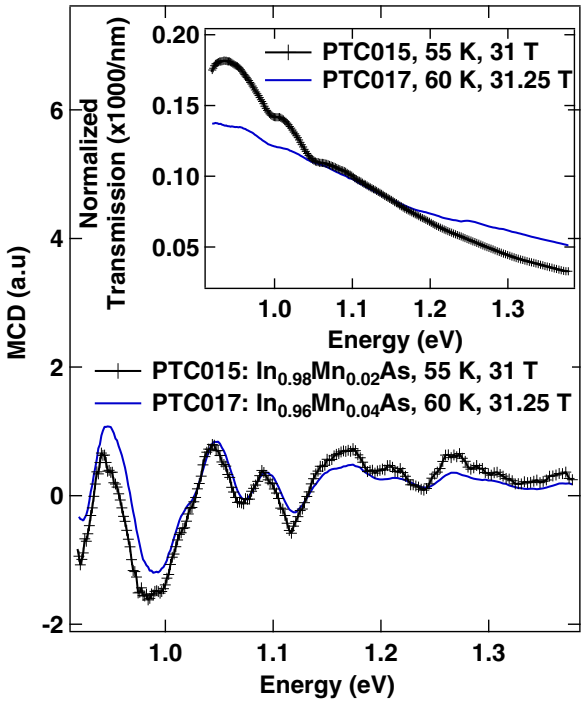

FIG. 5. (Color online) The MCD spectra of InMnAs with 2% and 4% Mn contents at 55 K, 31 T and 60 K, 31.25 T, respectively. At lower energies, the peaks are more distinct, however, as the excitation energy increases, the peaks start to convolute. The inset shows the transmissions through the samples at fixed magnetic fields.

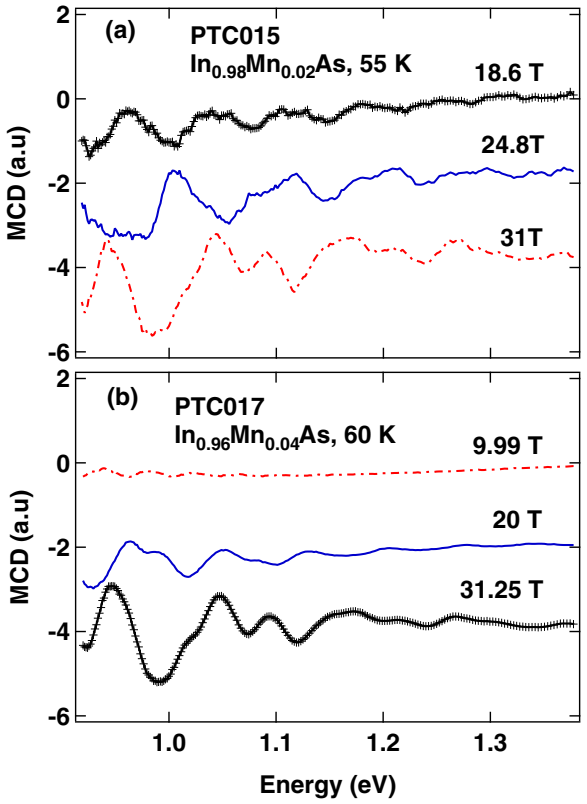

FIG. 6. (Color online) (a) The field dependance of MCD for $In_{0.98}Mn_{0.02}As$. As the field increases, the lowest energy peak at 18.6 T starts to blue shift and becomes more asymmetric. As the field is increased further, the peak blue shifts and starts to form a double structure. (b) The field dependance of $In_{0.96}Mn_{0.04}As$. Similar to the $In_{0.98}Mn_{0.02}As$, the evolution of MCD response, with increasing the field, shows blue shifts and the formation of double peaks.

contents. While the various maxima and minima are distinct at lower energies (0.92–1.1 eV), when examining the field dependence of the MCD response in Fig. 6, the peaks start to become more asymmetric and finally, as the field increases to 31 T, the splitting of the peaks is more distinct.

IV. THEORETICAL CALCULATIONS AND MODELING

Our theoretical model is based on an eight-band $\mathbf{k}\cdot\mathbf{p}$ Pidgeon-Brown model [30] for a narrow gap semiconductor in a static magnetic field parallel to the z-direction B_z. Elements of the model have been described in great detail elsewhere [31–34]. Here, we summarize the salient features of the model. In our model, since these are three dimensional, bulk systems, the wave vector k_z in the direction of the magnetic field is still a good quantum number and we include the full (k_z) wave vector dependence of the itinerant electronic states. We also allow for the sp-d coupling of the itinerant conduction band electrons and valence band holes to the localized d electrons in the Mn ion cores. We separate the eight Bloch basis states into an upper and lower set of four Bloch basis states, which decouple at the zone center, i.e., $k_z = 0$. The Bloch basis states for the upper set are $|S\uparrow\rangle$, $|HH\uparrow\rangle$, $|LH\downarrow\rangle$, and $|SO\downarrow\rangle$, which correspond to electron spin up, heavy-hole spin up, light-hole spin down, and split-off hole spin down, respectively. Similarly, the Bloch basis states for the lower set are $|S\downarrow\rangle$, $|HH\downarrow\rangle$, $|LH\uparrow\rangle$, and $|SO\uparrow\rangle$ corresponding to electron spin down, heavy-hole spin down, light-hole spin up, and split-off hole spin up. The explicit expressions for these eight Bloch basis states are given in Refs. [31–33]. The total effective mass Hamiltonian is the sum of the Landau (H_L), Zeeman (H_Z), and sp-d exchange ($H_{\rm ex}$) contributions, i.e.,

$$H = H_L + H_Z + H_{\rm ex} \tag{1}$$

Explicit expressions for these Hamiltonians are given in Refs. [31–33]. The parameters that we use for the model are given in Table II.

We used the standard Luttinger parameters [27] and temperature-dependent energy gaps for InSb and InAs as inputs in the Landau and Zeeman Hamiltonians. In the Mn exchange Hamiltonian, $H_{\rm ex}$, of Eq. (1), we follow the method of Kossut [35] and include the effects of the spontaneous magnetization of the Mn ions (magnetic impurities) and the coupling of this magnetization to the conduction band electrons and valence band holes through the s-d and p-d exchange interactions. The values of the exchange constants for the s-d interaction, $N_0\alpha$, and p-d interaction, $N_0\beta$, are taken to be -0.5 and 1.0 eV, respectively [36]. The spontaneous magnetization depends on the Mn concentration x, and the z component of the average Mn spin $\langle S_z\rangle$. In determining the z component of Mn spin, we can allow for the system to be either paramagnetic or ferromagnetic, this is described in Refs. [9,37]. The spin of the Mn ions is calculated using

TABLE II. Material parameters for InMnAs and InMnSb Ref. [27].

Parameter	InMnAs	InMnSb
Energy gap		
E_g^Γ(eV, $T=0$)	0.417	0.235
Electron effective mass		
m_e^*/m_0 ($T=0$)	0.026	0.0135
Luttinger parameters		
γ_1^L	20.0	34.8
γ_2^L	8.5	15.5
γ_3^L	9.2	16.5
Spin-orbit splitting		
Δ (eV)	0.39	0.81
Optical matrix parameters		
E_p (eV)	21.5	23.3
s-d and p-d exchange energies (eV)		
$N_0\alpha$	-0.5	-0.5
$N_0\beta$	1.0	1.0

mean-field theory, with $\langle S_z\rangle$ determined from

$$\langle S_z\rangle = SB_s\left\{\frac{gS}{kT}\left[\mu_B B - \frac{3kT_c\langle S_z\rangle}{gS(S+1)}\right]\right\}, \qquad (2)$$

where g is the free electron g factor, B_s is the Brillouin function, and $S=5/2$ is the spin of the magnetic Mn ion. The temperature T and the T_c depend on the measurements and the samples.

The values of x in our calculations are taken to be the Mn fraction in the actual samples as experimentally reported. The value of $\langle S_z\rangle$ is determined in the mean-field approximation using the lattice temperature T and the Curie temperature T_c of the samples from Table I as inputs. With the inclusion of ferromagnetic ordering of the Mn ions, the spontaneous magnetization and its *sp-d* coupling to the itinerant carriers will spin split the bands even in the absence of an external magnetic field.

In calculating the electronic structure with B $\neq$ 0, to simplify the results, we make the *axial approximation* where we replace γ_2 and γ_3 by their average $(\gamma_2+\gamma_3)/2$. This decouples the Pidgeon-Brown manifolds meaning that the Landau levels can be obtained by diagonalizing an 8×8 Hamiltonian (or smaller) for each Pidgeon-Brown manifold. For $B=0$, we do not need to make this approximation and we can view the full anisotropic bands. This is shown Fig. 7(a) for InMnSb and Fig. 8(a) for InMnAs, where we plot the bands for $B=0$ and $T=15$ K in both the [001] and [111] directions. We see that the bands are already spin-split even without the application of an external magnetic field since the two samples are ferromagnetic. In Figs. 7(b) and 8(b), we plot the Landau levels as a function of k_z for the InMnSb and InMnAs samples, respectively. In each figure, the red lines represent the transitions that are possible for 1.0-eV excitation and the blue lines represent the transitions possible for 1.5-eV excitation. We see that for 1.0 eV excitation, the SO to CB transition is not energetically possible, but it is possible once the excitation energy reaches the band gap between the SO and CB gap, which occurs below 1.1 eV (green line). This is

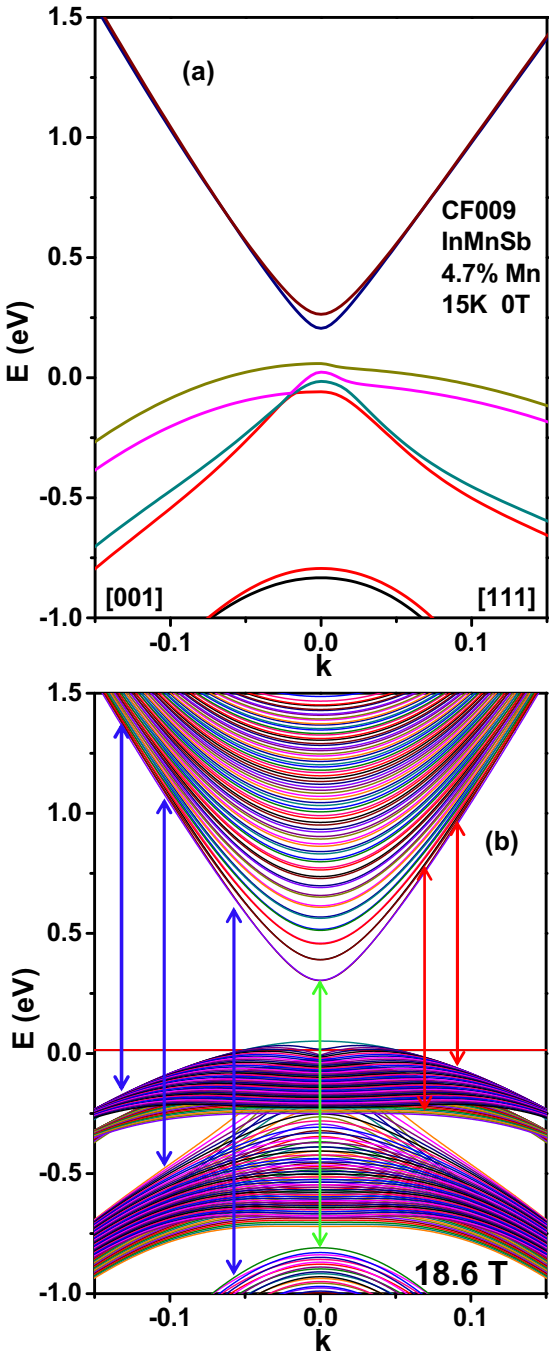

FIG. 7. (Color online) The electronic structure for InMnSb (with Mn = 4.7%) at 15 K (sample CF009). (a) Electronic structure with $B=0$ in the [001] and [111] direction. The bands are spin split owing to the ferromagnetism of the sample. (b) The electronic structure for $B=18.6$ T as a function of k_z showing the Landau levels structure. Red arrows show the approximate allowed transitions for excitation with a 1.0 eV and the blue arrows show the allowed transitions for a 1.5-eV excitation. We see that the SO to CB is not possible for 1.0-eV excitation. This transition first becomes allowed below 1.1 eV (green arrow).

in contrast to InMnAs where the SO split transition is possible for 1.0-eV excitation (even though the band gap is larger for InMnAs than for InMnSb, the SO splitting is smaller, and hence the SO to CB transition occurs at a smaller energy).

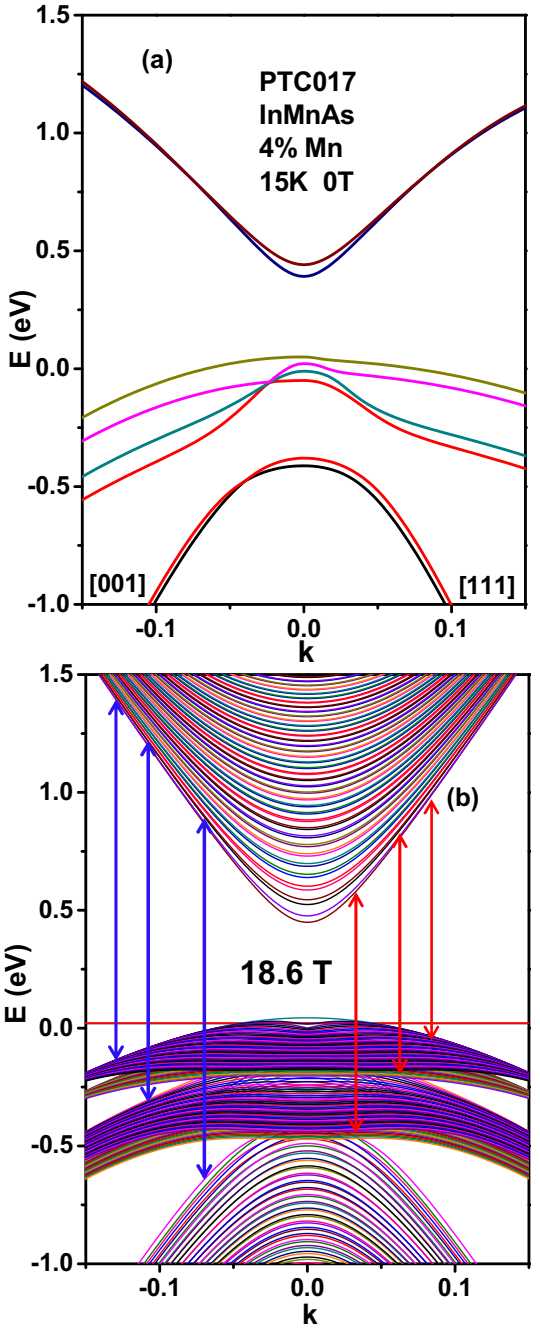

FIG. 8. (Color online) The electronic structure for InMnAs (with 4.0% Mn) at 15 K (sample PTC017). (a) Electronic structure with $B = 0$ in the [001] and [111] direction. The bands are spin-split owing to the ferromagnetism of the sample. (b) The electronic structure for $B = 18.6$ T as a function of k_z showing the Landau levels structure. Red arrows show the approximate allowed transitions for a 1.0-eV excitation and the blue arrows show the allowed transitions for a 1.5-eV excitation. Unlike InMnSb, we see that the SO to CB transition *is allowed* for a 1.0-eV excitation. While the band gap for InMnAs is larger than for InMnSb, the SO splitting Δ is smaller and thus the SO to CB transition is allowed at 1.0 eV.

We note that at $k_z = 0$, we can calculate the *relative strengths* of the valence band to conduction band transitions for circularly polarized light. This is shown in Table III. From the wave functions given in the table, we see that the ratio of the squares of the matrix elements (which gives the relative strengths of the transitions) for the HH, SO, and LH to CB transitions, for circularly polarized lights are 3 : 2 : 1, with the SO and LH transitions producing an opposite CB spin polarization than the HH transition. In the table, P is the momentum matrix element $P \equiv \langle S|P_x|X\rangle = \langle S|P_y|Y\rangle = \langle S|P_z|Z\rangle$.

TABLE III. Relative strength of the valence band to conduction band transitions for circularly polarized light.

Circ. Pol.	Hole State	Conduction Band state	Transition Strength
	$\|HH\uparrow\rangle$	$\|C\uparrow\rangle$	P^2
	$\frac{1}{\sqrt{2}}\|(X+iY)\uparrow\rangle$	$\|S\uparrow\rangle$	
	$\|LH\uparrow\rangle$	$\|C\downarrow\rangle$	$\frac{1}{3}P^2$
σ^-	$\frac{i}{\sqrt{6}}\|(X+iY)\downarrow - 2Z\uparrow\rangle$	$\|S\downarrow\rangle$	
	$\|SO\uparrow\rangle$	$\|C\downarrow\rangle$	$\frac{2}{3}P^2$
	$\frac{1}{\sqrt{3}}\|(X+iY)\downarrow + Z\uparrow\rangle$	$\|S\downarrow\rangle$	
	$\|HH\downarrow\rangle$	$\|C\downarrow\rangle$	P^2
	$\frac{i}{\sqrt{2}}\|(X-iY)\downarrow\rangle$	$\|S\downarrow\rangle$	
	$\|LH\downarrow\rangle$	$\|C\uparrow\rangle$	$\frac{1}{3}P^2$
σ^+	$\frac{1}{\sqrt{6}}\|(X-iY)\uparrow + 2Z\downarrow\rangle$	$\|S\uparrow\rangle$	
	$\|SO\downarrow\rangle$	$\|C\uparrow\rangle$	$\frac{2}{3}P^2$
	$\frac{-i}{\sqrt{3}}\|(X-iY)\uparrow + Z\downarrow\rangle$	$\|S\uparrow\rangle$	

To determine the optical properties, we use Fermi's golden rule to calculate the magneto-absorption. The absorption can be calculated for both σ^+ and σ^- circularly polarized light and if we subtract the two contributions, $\alpha_{\sigma^+} - \alpha_{\sigma^-}$, we can generate the MCD response. Figure 9 shows the comparison of the experimental MCD and the model for the two InMnSb films. We assigned the first transitions, below 1.1 eV to the SO-CB, and the higher energy MCD responses, to several possible valence band transitions. The model described here provides a better fit to the film with 4.7% compared to the film with 10% Mn content.

Figure 10 shows the magnetic field evolution of the MCD for the InMnAs film with 2% Mn content from 12.4 to 31 T. The small features grow as the magnetic field increases and our model maps even these observed small features. As summarized in Table II, the *s-d* and *p-d* coupling parameters are kept the same for both InMnAs and InMnSb and the other parameters were selected from the accepted parameters for bulk InSb and InAs. The broadenings in the transitions were used as an input parameter.

V. TEMPERATURE DEPENDENCE

A. InMnAs

Aside from the magnetic-field-dependence measurements, the temperature dependence was also taken as shown in Fig. 11. In Fig. 11, the MCD was normalized by the value of the MCD at 0.992 eV for both samples (the traces are shifted for clarity after the normalization). Since the transition probability is independent of temperature, the MCD should scale with temperature if it originates only from one transition. Therefore, if the MCD is normalized by the MCD at a

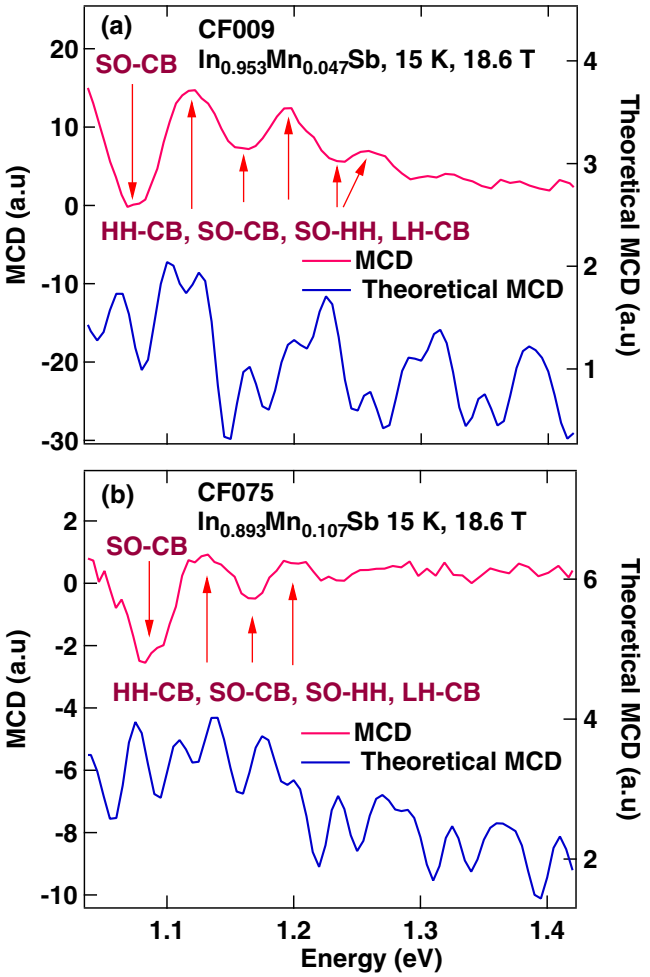

FIG. 9. (Color online) The theoretical model and the experimental MCD responses of the two InMnSb films, CF009 and CF075 at 15 K and 18.6 T. The model can describe the features in the (a) for 4.7% Mn content better than the sample with 10% Mn in (b).

certain point, we should be able to determine if each peak is the result of a single or multiple transitions [16,38]. The normalized MCD shown in Figs. 11(a) and 11(b), clearly demonstrates the shifts in the individual peak position, thus the peaks are due to a composition of a response from multiple transitions. This temperature dependence has been reflected both in the experimental observation and the presented model in Fig. 10. Earlier studies reported in Ref. [16] observed a similar temperature dependence of their main observed MCD transitions in an MOVPE grown InMnAs.

B. InMnSb

As stated earlier, if the MCD is caused by a single transition, then the temperature dependence would only scale the spectra, whereas a shift in the peak position could be the consequence of multiple transitions [15,38]. This process can be seen in the transition from Fig. 12(a) to Fig. 12(b); the latter presents the MCD of the InMnSb with 4.7% Mn (CF009) normalized to its value at 1.117 eV (the traces are shifted for clarity after the normalization). As the MCD spectra clearly show more complex behavior than scaling, the resulting MCD is due to

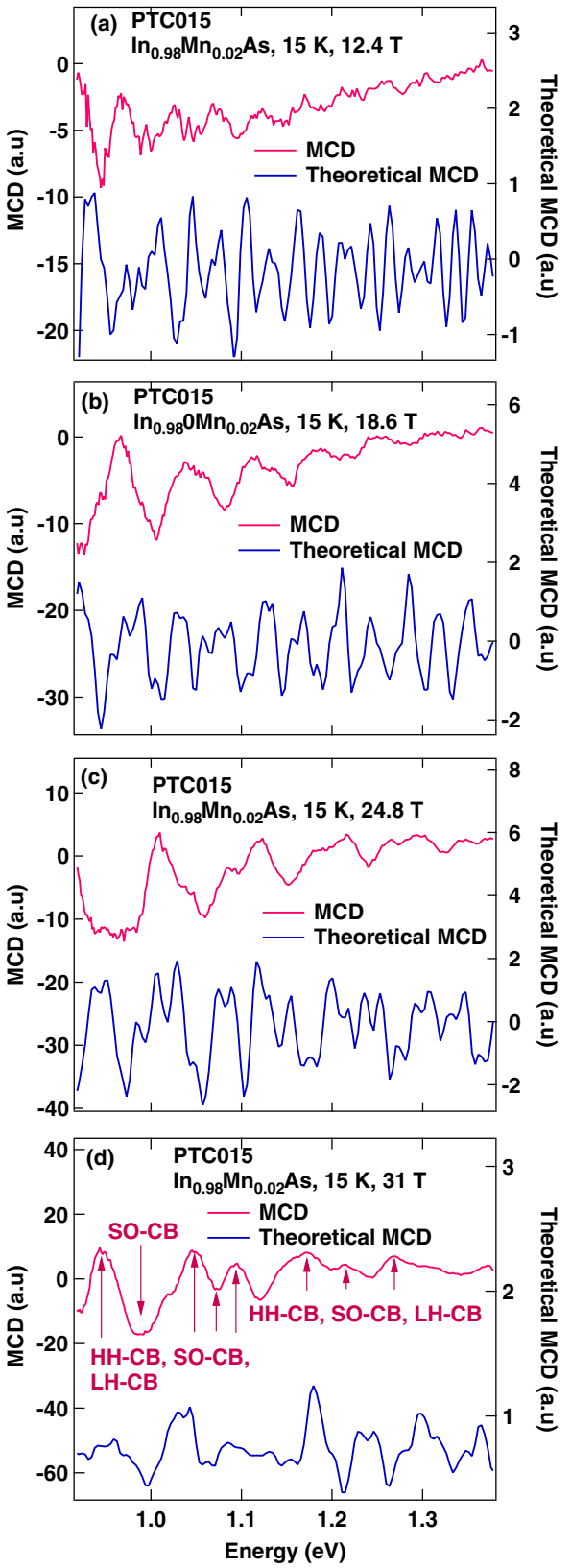

FIG. 10. (Color online) A comparison between the theoretical MCD (blue) and experimental MCD (red) at 15 K and (a) 12.4, (b) 18.6, (c) 24.8, and (d) 31 T. The theoretical MCD matches the observed MCD features, the broadening of the transitions was adjusted to provide the best fit. The small features grow as the magnetic field increases and our model maps this evolution accurately.

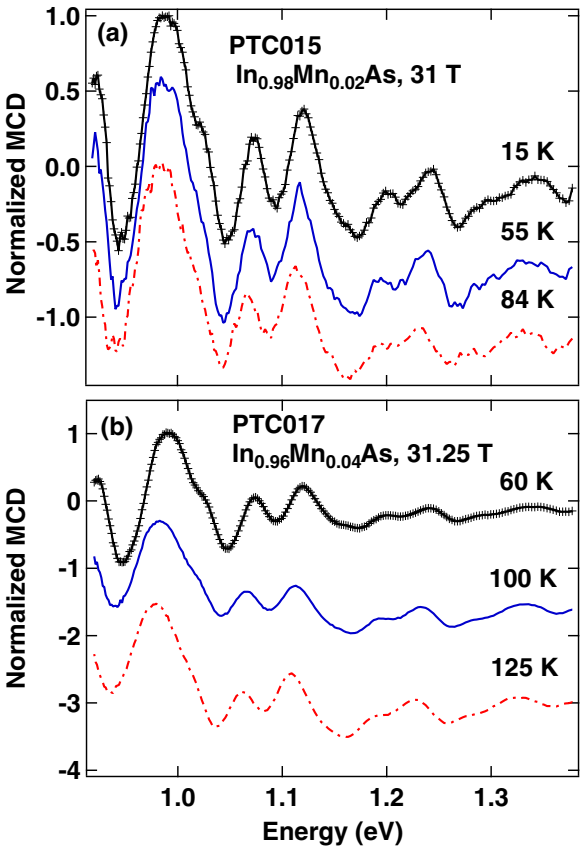

FIG. 11. (Color online) Temperature dependence of (a) $In_{0.98}Mn_{0.02}As$ at 31 T and (b) $In_{0.94}Mn_{0.04}As$ at 31.25 T. In order to determine whether each peak is due to a single or multiple transitions, we normalized the MCD to the value of the MCD at 0.992 eV. For both samples, the peaks shift with temperature implying that the individual peaks are due to multiple transitions, as the temperature dependence of the band gaps cannot entirely explain the shifts.

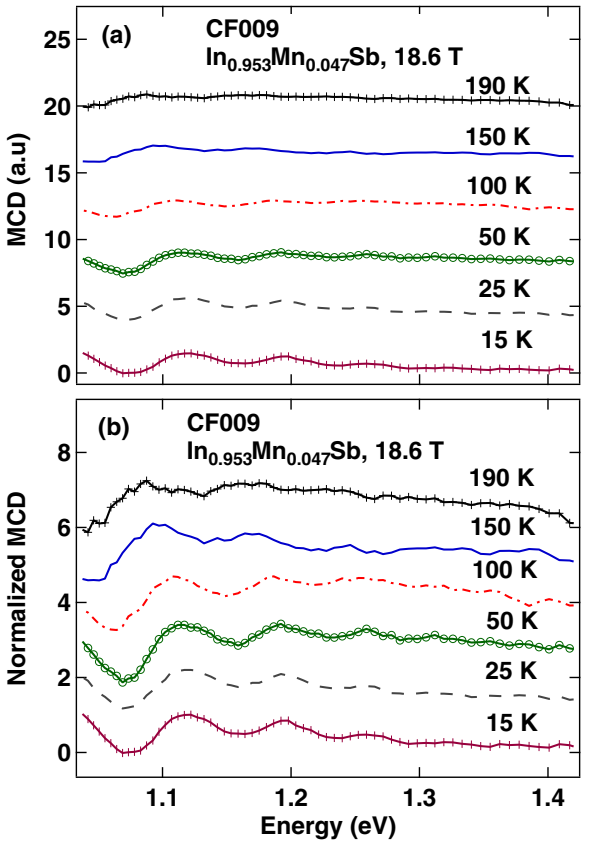

FIG. 12. (Color online) (a) The temperature dependence of the InMnSb sample (CF009) with 4.7% Mn at 18.6 T. (b) In order to determine if the MCD is comprised of a single or multiple transitions, the MCD at each temperature was normalized to the MCD at 1.117 eV. The temperature dependence of the band gaps cannot entirely explain the shifts in the individual peaks.

multiple transitions where our excitation energy range allowed multiple transitions from the valence bands to the CB. This is supported by a theoretical model in which multiple transitions can be seen near each of the observed peaks. Furthermore, the peak at ∼1.08 eV at 15 K and 18.6 T for the CF009 sample originate from SO-CB transitions. A similar normalization was done for the MCD response of the sample with 10.7% Mn, as shown in Fig. 13(b), where in order to determine if the MCD is comprised of a single or multiple transitions, the MCD responses in Fig. 13(a), at each temperature, were normalized to the MCD at 1.069 eV (the traces are shifted for clarity after the normalization).

VI. SO-CB GAP AND VARSHNI COEFFICIENTS

The MOVPE grown InMnSb samples have a large peak below 1.1 eV and the InMnAs samples have a large peak below 1 eV at ∼15 K and 18.6 T. We assign these peaks to the SO to CB transitions, which is at 1.045 eV at 0 K for InSb and 0.807 eV for InAs [27]. One might question why we assign this to the SO-split rather than the HH-band transition, since the HH transition is stronger, according to Table II. It is important to note though, that the results in Table II hold only for the $k = 0$ basis functions of the state. Away from $k = 0$, band-mixing effects can decrease the strength of the transitions. Our band structure calculations suggest that only one valence band (corresponding to the $p = -1$ Pidgeon-Brown manifold) is a pure HH state, corresponding to the $n = 0$ Landau level, for the HH spin-down state. When one goes to higher Landau levels (even at $k = 0$), there is strong mixing between the HH and LH, which reduces the strength of the transitions. In addition, as one goes to higher excitation energy, the transitions occur for larger and larger values of k_z, which also increases the mixing. Also, there is a *density of states* effect (for the one-dimensional density of states associated with the k_z quantum number in the direction of the magnetic field), which varies as $1/\sqrt{(E)}$ or $1/k$ and makes the $k = 0$ transitions the strongest. We note that in contrast to the HH and LH transitions, the SO transition initially occurs when $k = 0$ and these states are almost pure SO states and have less mixing, i.e., they are ∼98% SO. Mixing is also less for the SO states since they are not initially degenerate with the LH and HH states. Finally, we also point out that the initial HH and LH Landau levels (near $k = 0$) lie above the Fermi level so these transitions are not possible.

By assigning the peak at ∼1.08 eV at 18.6 T, 15 K for InMnSb (CF009) to the SO to CB transition, we can use the magnetic field and temperature dependence to extract the

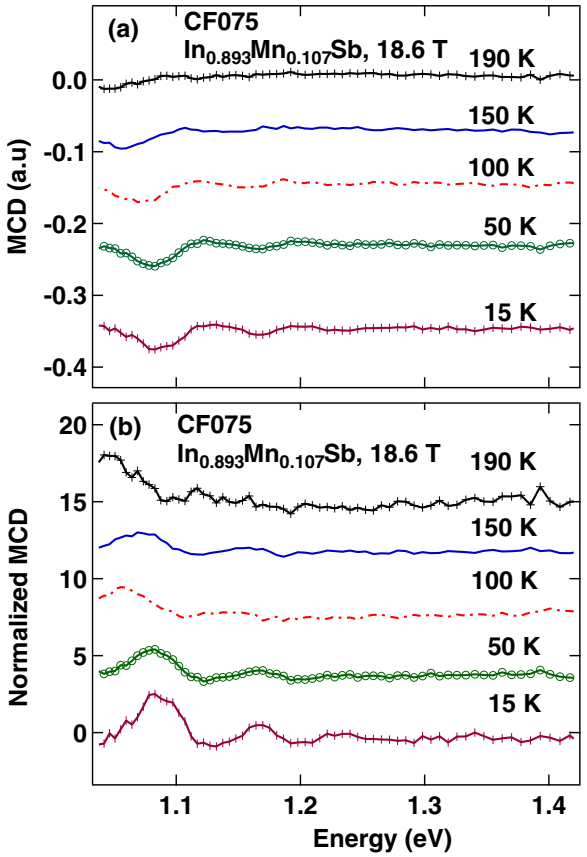

FIG. 13. (Color online) (a) The temperature dependence of the InMnSb sample (CF075) with 10.7% Mn at 18.6 T. (b) In order to determine if the MCD is comprised of a single or multiple transitions, the MCD at each temperature was normalized to the MCD at 1.069 eV.

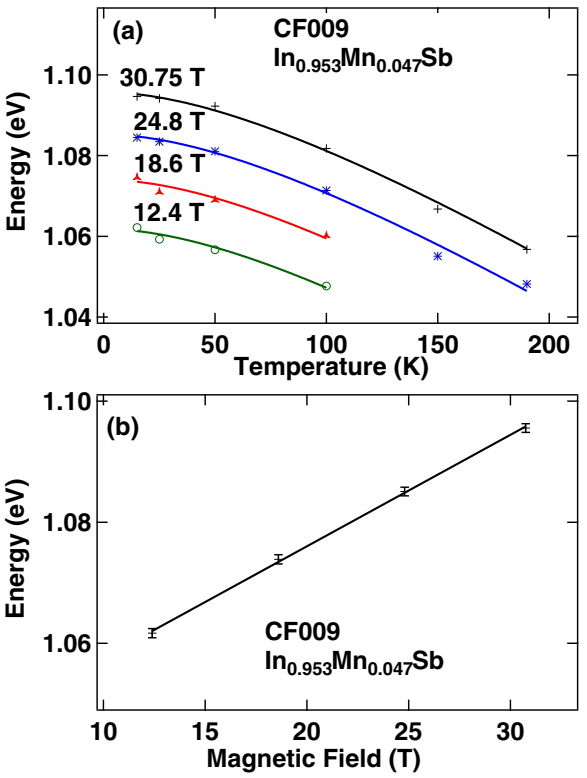

FIG. 14. (Color online) In order to find the SO to CB gap, we fit the evolution of the peak at ∼1.07 eV at 15 K at 18.6 T, for InMnSb (CF009, 4.7% Mn), at various temperatures and magnetic fields. As shown in (a) the temperature dependence of the transition was fit to the Varshni equation, with the constraints that A and B were the same for all of the fields. (b) These gaps were plotted vs the magnetic fields and from a linear fit the gap of 1.0392 ± 0.00075 eV at zero field can be estimated.

gap between the SO band and the CB. An example of the magnetic field dependence at 15 K is shown earlier in Fig. 3. As expected, the peak's amplitude increases and the peak blue shifts with increasing field. The peak position was calculated by a Gaussian fit, and the position for each magnetic field was plotted versus temperature in Fig. 14(a). Similar to the modeling of the fundamental gap, the points were fit to the Varshni equation $E_g(0) = E_g(T) + \frac{AT^2}{B+T}$, with A and B being 0.37 meV/K and 155 K, respectively. These values are close to the recommended values from Ref. [27] to be 0.32 meV/K and 170 K. As shown in Fig. 14(b), the resulting SO gaps were plotted as a function of the magnetic field and fit to a line, giving a y intercept of 1.039 ± 0.00075 eV, which is close to the expected 1.045 eV SO gap in bulk InSb. We used the same procedure for the InMnAs, and Table IV summarizes the extracted SO-CB gaps as well as the Varshni coefficients for InMnSb and InMnAs.

VII. CONCLUSIONS

The large g factors in the narrow gap InMnSb and InMnAs systems allow us to measure the MCD at relatively high temperatures. Our experimental measurements were compared with MCD calculations based on an eight-band Pidgeon-Brown model extended to include the effects of the Mn impurities and the sp-d exchange interaction and allowed for ferromagnetic order of the Mn ions. A comparison of our experimental and theoretical results shows that the dominant structure in the MCD spectrum *in this energy range* comes from the *split-off hole to conduction band transitions.* This is somewhat surprising since one usually thinks of the HH to CB band as being a stronger transition. In this case, the SO to CB transition was the strongest for a variety of reasons: (i) as shown in Figs. 7 and 8 in this energy range, the HH and LH band transitions occur in the higher Landau levels and also away from $k_z = 0$. As a result, HH and LH transition states are heavily mixed. (ii) For k_z away from 0, there is a density of states effect, which decreases the strength of the transition. (iii) The SO transition occurs near $k_z = 0$, where there is little

TABLE IV. The spin-orbit (SO) to conduction-band (CB) gap and the Varshni coefficients (A and B) in InMnSb and InMnAs compared to InSb and InAs.

Sample	$E_{SO->CB}(0)$ (eV)	A (meV/K)	B (K)
$In_{0.953}Mn_{0.047}Sb$	1.0392 ± 0.0012	0.37± 0.06	155± 56
InSb, Ref. [27]	1.045	0.32	170
$In_{0.98}Mn_{0.02}As$	0.85635	0.18	137
InAs, Ref. [27]	0.807	0.276	93

TABLE V. The temperature dependent of Δg for InMnSb and InMnAs.

Temperature (K)	InMnSb Mn = 4.7% Δg	InMnSb Mn = 10% Δg	InMnAs Mn = 2% Δg
15	31.9	46.3	86.4
25	31.55		
50	31.7	26.75	
55			78.0
84			81.8
100	30.91		
150	28.27		
190	29.06		

mixing. In addition, we do not identify any transitions that could be associated with the impurity bands.

From our band structure calculations, it can be seen that the SO-CB transition occurs at an energy slightly higher (lower) than 1.0 eV for InMnSb (InMnAs). The largest peak for InMnSb (at ∼1.08 eV at 15 K and 18.6 T) was fit to the Varshni equation, which leads to parameters close to the earlier reported values for InSb [27]. Since for InMnSb the SO-CB transition dominates, we were able to use the field dependence of the largest transition peak (SO → CB) to extract the difference in the g factor between the SO and CB bands. In order to find the difference in g factor, the peak position of each sample, at a given temperature, was plotted as a function of the magnetic field. The peak positions were fit to the equation $\mathrm{E} = \Delta g \mu \mathrm{B} + E_0$, where E is the peak position at different fields, Δg is the difference in the CB and SO g factors, μ is the Bohr magneton, and E_0 is the SO-CB gap at zero magnetic field. Due to the limits in our energy range, the Δg for $In_{0.96}Mn_{0.04}As$ could not be determined. The resulting values for the other three samples are summarized in Table V. The Δg factor is relatively constant throughout the temperature range for $In_{0.953}Mn_{0.047}Sb$.

ACKNOWLEDGMENTS

This work was supported by the AFOSR through Grant FA9550-14-1-0376. In addition, (GK,BM,MM) were supported by NSF-Career Award DMR-0846834 and (BW) was supported by NSF-DMR-60035274 and NSF-DMR-1305666. S.M. acknowledges support from the NSF MRI program (DMR-1229217). A portion of this work was performed at the National High Magnetic Field Laboratory, which is supported by National Science Foundation Cooperative Agreement No. DMR-1157490 and the State of Florida.

M.A.M. and B.A.M. have contributed equally to this work.

[1] T. Wojtowicz, G. Cywinski, W. L. Lim, X. Liu, M. Dobrowolska, J. K. Furdyna, K. M. Yu, W. Walukiewicz, G. B. Kim, M. Cheon, X. Chen, S. M. Wang, and H. Luo, Appl. Phys. Lett. **82**, 4310 (2003).

[2] T. Wojtowicz, W. L. Lim, X. Liu, G. Cywinski, M. Kutrowski, L. V. Titova, K. Yee, M. Dobrowolska, J. K. Furdyna, K. M. Yu, W. Walukiewicz, G. B. Kim, M. Cheon, X. Chen, S. M. Wang, H. Luo, I. Vurgaftman, and J. R. Meyer, Physica E **20**, 325 (2004).

[3] M. Tanaka, S. Ohya, and P. N. Hai, App. Phys. Rev. **1**, 011102 (2014).

[4] M. Tanaka and S. Ohya, *Spintronic Devices Based on Semiconductors in Comprehensive Semiconductor Science and Technology*, edited by P. Bhattacharya, R. Fornari, and H. Kamimura (Elsevier, Amsterdam, 2011), Vol. 6, pp. 540–562.

[5] H. Ohno, A. Shen, F. Matsukura, A. Oiwa, A. Endo, S. Katsumoto, and H. Iye, Appl. Phys. Lett. **69**, 363 (1996).

[6] G. A. Khodaparast, R. E. Doezema, S. J. Chung, K. J. Goldammer, and M. B. Santos, Phys. Rev. B **70**, 155322 (2004).

[7] M. Frazier, J. G. Cates, J. A. Waugh, J. J. Heremans, M. B. Santos, X. Liu, and G. A. Khodaparast, J. Appl. Phys. **106**, 103513 (2009).

[8] O. Olendski, Q. L. Williams, and T. V. Shahbazyan, Phys. Rev. B **77**, 125338 (2008).

[9] M. Bhowmick, T. R. Merritt, G. A. Khodaparast, B. W. Wessels, S. A. McGill, D. Saha, X. Pan, G. D. Sanders, and C. J. Stanton, Phys. Rev. B **85**, 125313 (2012).

[10] H. Munekata, H. Ohno, S. von Molnar, A. Segmuller, L. L. Chang, and L. Esaki, Phys. Rev. Lett. **63**, 1849 (1989).

[11] H. Ohno, H. Munekata, S. von Molnar, and L. L. Chang, J. Appl. Phys. **69**, 6103 (1991).

[12] A. J. Blattner and B. W. Wessels, Appl. Surf. Sci. **221**, 155 (2004).

[13] N. Rangaraju, P. Li, and B. W. Wessels, Phys. Rev. B **79**, 205209 (2009).

[14] N. D. Parashar, N. Rangaraju, V. K. Lazarov, S. Xie, and B. W. Wessels, Phys. Rev. B **81**, 115321 (2010).

[15] P. T. Chiu and B. W. Wessels, Appl. Phys. Lett. **89**, 102505 (2006).

[16] P. T. Chiu and B. W. Wessels, Phys. Rev. B **76**, 165201 (2007).

[17] G. A. Khodaparast, Y. H. Matsuda, D. Saha, G. D. Sanders, C. J. Stanton, H. Saito, S. Takeyama, T. R. Merritt, C. Feeser, B. W. Wessels, X. Liu, and J. Furdyna, Phys. Rev. B **88**, 235204 (2013).

[18] M. Wang, R. A. Marshall, K. W. Edmonds, A. W. Rushforth, R. P. Campion, and B. L. Gallagher, Appl. Phys. Lett. **104**, 132406 (2014).

[19] A. Winter, H. Pascher, H. Krenn, T. Wojtowicz, X. Liu, and J. K. Furdyna, AIP Proc. **893**, 1223 (2007).

[20] A. Winter, H. Pascher, M. Hofmayer, H. Krenn, T. Wojtowicz, X. Liu, and J. Furdyna, Rev. Adv. Mater. Sci. **20**, 92 (2009).

[21] C. Thurn, V. M. Axt, A. Winter, H. Pascher, H. Krenn, X. Liu, J. K. Furdyna, and T. Wojtowicz, Phys. Rev. B **80**, 195210 (2009).

[22] T. Schallenberg and H. Munekata, Appl. Phys. Lett. **89**, 042507 (2006).

[23] A. J. Blattner, P. L. Prabhumirashi, V. P. Dravid, and B. W. Wessels, J. Cryst. Growth. **259**, 8 (2003).

[24] Y. L. Soo, S. Kim, Y. H. Kao, A. J. Blattner, B. W. Wessels, S. Khalid, C. Sanchez Hanke, and C.-C. Kao, Appl. Phys. Lett. **84**, 481 (2004).
[25] Leonardo Lari, Stephen Lea, Caitlin Feeser, Bruce W. Wessels, and Vlado K. Lazarov, J. Appl. Phys. **111**, 07C311 (2012).
[26] Caitlin E. Feeser, Leonardo Lari, Vlado K. Lazarov, John A. Peters, and Bruce W. Wessels, J. Vac. Sci. Technol. B **30**, 032801 (2012).
[27] I. Vurgaftman, J. R. Meyer, and L. R. Ram-Mohan, J. Appl. Phys. **89**, 5815 (2001).
[28] M. Dobrowolska, K. Tivakornsasithorn, X. Liu, J. K. Furdyna, M. Berciu, K. M. Yu, and W. Walukiewicz, Nat. Mater. **11**, 444 (2012).
[29] N. D. Parashar, P. T. Chiu, and B. W. Wessels, Physica E **41**, 1147 (2009).
[30] C. K. Pidgeon and R. N. Brown, Phys. Rev. **146**, 575 (1966).
[31] G. D. Sanders, Y. Sun, C. J. Stanton, G. A. Khodaparast, J. Kono, Y. H. Matsuda, N. Miura, T. Slupinski, A. Oiwa, and H. Munekata, J. Appl. Phys. **93**, 6897 (2003).
[32] G. D. Sanders, Y. Sun, C. J. Stanton, G. A. Khodaparast, J. Kono, Y. H. Matsuda, N. Miura, T. Slupinski, A. Oiwa, and H. Munekata, J. Superconductivity **16**, 449 (2003).
[33] G. D. Sanders, Y. Sun, C. J. Stanton, G. A. Khodaparast, J. Kono, D. S. King, Y. H. Matsuda, S. Ikeda, N. Miura, A. Oiwa, and H. Munekata, Physica E **20**, 378 (2004).
[34] Y. Sun, F. V. Kyrychenko, G. D. Sanders, C. J. Stanton, G. A. Khodaparast, J. Kono, Y. H. Matsuda, and H. Munekata, SPIN **5**, 1550002 (2015).
[35] J. Kossut, Semiconductors Semimetals **25**, 183 (1988).
[36] M. A. Zudov, J. Kono, Y. H. Matsuda, T. Ikaida, N. Miura, H. Munekata, G. D. Sanders, Y. Sun, and C. J. Stanton, Phys. Rev. B **66**, 161307(R) (2002).
[37] G. A. Khodaparast, J. Kono, Y. H. Matsuda, S. Ikeda, N. Miura, Y. J. Wang, T. Slupinski, A. Oiwa, H. Munekata, Y. Sun, F. V. Kyrychenko, G. D. Sanders, and C. J. Stanton, Physica E **21**, 978 (2004).
[38] B. Beschoten, P. A. Crowell, I. Malajovich, D. D. Awschalom, F. Matsukura, A. Shen, and H. Ohno, Phys. Rev. Lett. **83**, 3073 (1999).